

## SEVERE PLASTIC DEFORMATION OF METALS

BERT VERLINDEN

*Katholieke Universiteit Leuven, Department of Materials Engineering Kasteelpark  
Arenberg 44, B-3001 Heverlee, Belgium, Bert.Verlinden@mtm.kuleuven.ac.be*

### ABSTRACT

This paper provides an introduction in the field of severe plastic deformation (SPD). First of all the main methods to produce SPD materials are discussed. In the following section, the mechanisms leading to the formation of fine grains are reviewed and the influence of changes in strain path is highlighted. During post-SPD thermal annealing, some typical microstructural changes take place. The influence of SPD and subsequent annealing on strength, ductility and superplastic properties are reviewed. Finally the paper provides a short overview of fatigue resistance and corrosion properties of those materials.

**Keywords:** severe plastic deformation (SPD), submicron grains, equal channel angular pressing (ECAP)

### INTRODUCTION

Since the pioneering work of Hall [1] and Petch [2], material scientists and engineers have been attracted by materials with small grain sizes. A finer grain size increases the strength and the fracture toughness of the material and provides the potential for superplastic deformation at moderate temperatures and high strain rates. Traditional thermo-mechanical processes generally leads to a grain size above 10 $\mu$ m or, exceptionally, a few microns in diameter. However, several techniques to obtain submicron or nano-size grains are now available, e.g. vapor deposition, high-energy ball milling, fast solidification and severe plastic deformation (SPD). In the present paper we will explore the achievements and possibilities of the latter technique. Large plastic deformations can in principle be obtained by classical forming techniques like cold rolling and wire drawing. In a first approximation, not taking into account shear deformation at the surface, these techniques follow a continuous strain path and lead to a so-called ‘cellular’ or ‘fibrous’ substructure with many low angle boundaries [3][4]. However, specific SPD techniques, like those described in the next paragraph, offer the possibility to change the strain path during deformation. In the paragraph about “influence of strain path” it will be explained how this promotes the development of high angle boundaries and granular (sub)structures.

The goal of the present paper is to provide an introduction in the field of severe plastic deformation. For a deeper analysis of the subject the reader is referred to more extensive overviews e.g. Valiev [5], or to the proceedings of recent conferences on this subject<sup>1</sup>.

---

<sup>1</sup> The second and third Int. Conf. On Ultrafine Grained Materials, ed. Y.T. Zhu et. al., TMS (2002) and (2004).

## MAIN METHODS FOR SPD

Valiev [5] recently formulated three requirements to obtain materials with submicron grain size: the fine grained material must have predominantly high angle boundaries, the structure must be uniform over the sample volume and the large plastic strains may not have generated internal damage or cracks. Traditional deformation methods like rolling and wire drawing cannot meet these requirements. Therefore special deformation techniques have been developed. Probably the oldest, and certainly the most popular at this moment is the “Equal Channel Angular Pressing” (ECAP), also known as “Equal Channel Angular Extrusion” (ECAE). This technique has originally been developed by Segal et. al.[6][7]. A billet of the test material is pressed through a die consisting of two channels with identical cross sections, intersecting at an angle  $\phi$ , usually  $60^\circ < \phi < 135^\circ$  and often  $\phi = 90^\circ$  (fig. 1a). Some dies have a rounded corner with angle  $\psi$ , others have  $\psi = 0$ .

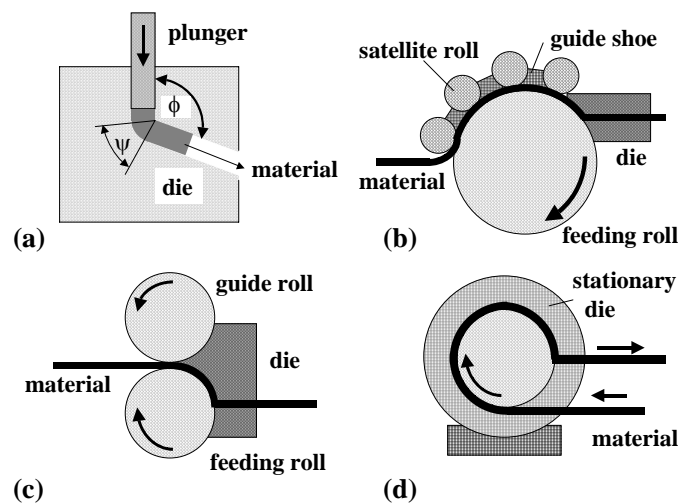


Fig. 1. Schematic illustrations of (a) a lab scale ECAP die; (b) the conshearing process [after 13]; (c) continuous confined strip shearing [after 14] and (d) the ECAP-conform set-up [after 15]

The deformation occurs by simple shear parallel to the intersecting plane of the channels. In theory, the shear is concentrated in a narrow band around this plane. However, FE simulations [8][9] and experiments with scribed grids [10] have shown that in practice the shear is spread over a deformation zone. The deformation is plane strain, since the strain in the TD direction is zero. The equivalent strain per pass depends on the angles  $\phi$  and  $\psi$  [11]:

$$\varepsilon_{eq} = 1/\sqrt{3}[2\cot(\psi/2 + \phi/2) + \psi \operatorname{cosec}(\psi/2 + \phi/2)] \quad (1)$$

For  $\psi = 0$  and  $\phi = 90^\circ$ ,  $\varepsilon_{eq} = 1.155$ . Because the channels have an identical cross section, the dimensions of the billet remain unchanged, and the process can in principle

be repeated any given number of times. If the cross section has a 4-fold symmetry axis, the sample can be rotated over  $90^\circ$  or  $180^\circ$  about the extrusion direction (ED) before reinsertion in the die.

Based on the regular repetition of such a rotation  $\phi$  around ED, four commonly applied routes have been defined. For route A,  $\phi$  is  $0^\circ$  (no rotation), for route C it is  $180^\circ$ , for route  $B_C$  it is  $90^\circ$ , and for route  $B_A$   $\phi$  is alternatively  $+90^\circ$  and  $-90^\circ$ . Note that via route C each volume element is restored to its initial shape after every  $2n$  passes and for route  $B_C$  after every  $4n$  passes, where  $n$  is an integer. From the point of view of dislocation activity, there is always a change of strain path between 2 ECAP passes. The nature of this change depends on the die angle  $\phi$  and the rotation angle  $\phi$ . The effect on microstructure and mechanical properties of the four routes, imposing different grain shape changes and different changes of strain path, will be discussed in next section. In general one can say that ECAP yields grain sizes of 300 – 500nm.

In spite of the actual popularity of the technique, some drawbacks of ECAP must be recognized. ECAP is a discontinuous process with limitations in up-scaling potential. Moreover, the volume fraction of useful material (with uniform microstructure and without cracks) can be rather low because only the portion of the billet that has passed through the shear zone, will receive the desired deformation and grain refinement. Barber et. al. figured out that for a sample with square cross section and an aspect ratio of 6, after 8 ECAP passes route A, only ~30% of the material is fully worked as intended. For route B, the efficiency is ~45% and for route C it is ~83% [12].

To increase the efficiency of ECAP, a number of continuous processes have recently been proposed. They combine the concept of ECAP with classical rolling. In the “*conshearing*” process [13] a large feeding roll and a number of smaller satellite rolls push a sheet into an ECAP die (fig 1b). Guide shoes in between the satellite rolls prevent buckling of the sheet. In “*continuous confined strip shearing*” (C2S2) [14], a specially designed feeding roll and a guide roll are used to feed a metal strip into the ECAP channel (fig. 1c). The initial sheet thickness is slightly reduced by the two rolls, but regains its initial thickness in the outlet of the ECAP die. In the “*ECAP-conform*” set-up, a groove in a central rotating shaft contains the work-piece (fig. 1d). Due to frictional forces the work-piece is driven into a second channel, like in ECAP. With this device an Al wire of 1 meter has been extruded several times, reducing the initial grain size from 5-7  $\mu\text{m}$  to the submicron level [15]. All these continuous techniques are still in an experimental stage, but they open perspectives for a more efficient production of fine-grained materials.

Rolling mills can also be used without ECAP attachment. In “*Accumulated Roll Bonding*” (ARB)[16] two sheets are stacked together and rolled simultaneously with 50% reduction (fig. 2). When the original contact surface has adequately been degreased and wire-brushed, the two sheets are bonded together (roll-bonding). The new sheet is divided in two parts and the whole sequence is repeated. The alignment of the sheets relative to each other can be changed after each cycle. For various materials including steel, aluminium alloys, copper and nickel, grain refinement down to the submicron level has been reported [17]. Nevertheless, considerable technological difficulties in the production of ARB samples have also been noticed. Edge cracks are frequently observed and the thickness reduction of the strip can be inhomogeneous [18].

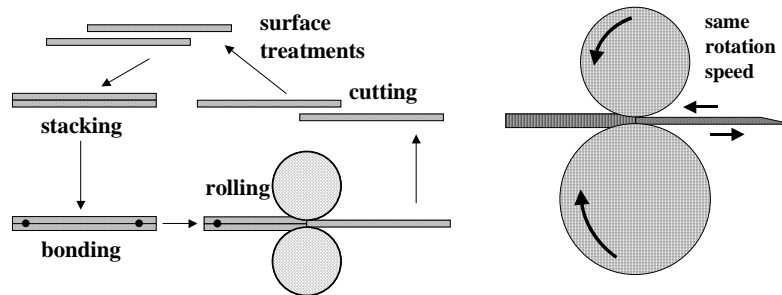


Fig. 2. Schematic illustration of accumulated roll bonding and asymmetric rolling

In “asymmetric rolling” the shear component on the sheet surface is enhanced as much as possible. This can be done using rolls with different diameter (fig. 2) or rolls with equal diameter but different rotation speed. Cui et. al. [19] obtained in high purity aluminium an average grain size of  $\sim 2\mu\text{m}$  after 90% reduction. The evolution of the structure during asymmetric rolling was attributed to the simultaneous action of compression and shear.

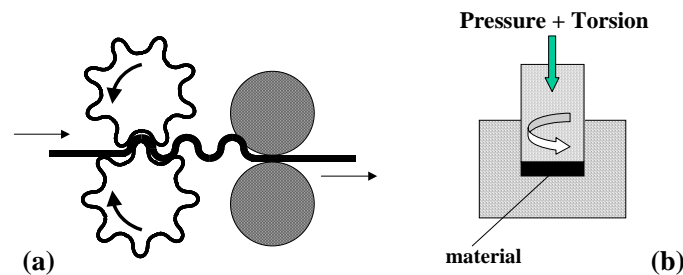


Fig. 3. Illustration of high-pressure torsion and continuous repetitive corrugation and straightening [after 20]

Other SPD techniques that have been proposed, rely upon the repetitive bending and straightening of a sheet. Several variants of this method have been proposed, like “repetitive corrugation and straightening” [20] (fig. 3a), “constrained groove pressing” [21] and “constrained groove rolling” [22]. Finally, one important lab-scale technique must certainly be mentioned: *high-pressure torsion* (HPT) (fig. 3b). Small discs (typically 10-20mm diameter and 0.2 – 1mm thick) are strained in torsion under an applied pressure of several GPa. Although in a classical torsion test it is generally assumed that the center of the sample is not deformed ( $\gamma = 2\pi RN/l$  with R the distance from the axis, N the number of turns and l the sample length), numerous investigations show that after several rotations the HPT-samples are uniform over the diameter [5], which shows that the real deformation in HPT is more complex than one can assume from the simple analytical expressions used in a classical torsion test. The main advantage of HPT is that extreme grain refinement (up to 100nm) can be obtained.

#### MICROSTRUCTURAL EVOLUTION DURING SPD

Grain refinement by severe plastic deformation implies the creation of new high angle grain boundaries (HAB). This can be accomplished by three mechanisms [4]. The first is the elongation of existing grains during plastic deformation, causing an increase

in high angle boundary area. The second is the creation of high angle boundaries by grain subdivision mechanisms. Finally an elongated grain can be split up by a localization phenomenon such as a shear band. The second mechanism is probably the most important one and merits some further explanations. The development of new boundaries inside an original grain by deformation has been known for several decades, probably since 1940 [23]. It has been described qualitatively in earlier review papers e.g. [3] and [4]. The possible mechanisms of formation have more recently been reviewed by Hughes and Hansen [24]. Grain subdivision starts at low to medium strains when grains break up in cells and cell blocks [25]. With increasing strain this substructure evolves towards a lamellar structure. During this process new high angle boundaries are generated. This happens by the simultaneous action of a microstructural and a texture mechanism [24]. The former starts at low deformations and consist in the accumulation of dislocations in the cell- and cell block boundaries in which the misorientations gradually increase with increasing strain. Some boundaries remain low angle boundaries but a significant fraction evolves into medium-high angle boundaries mostly in the range  $15^{\circ}$  -  $30^{\circ}$ . The texture mechanism involves the rotation of different parts of a subdivided grain towards different end orientations. This can generate very high misorientations in the range  $20^{\circ}$  -  $60^{\circ}$ .

When the deformation is applied following a continuous strain path, it will result in a fibrous structure with a relatively high fraction of low angle boundaries like it is often found in cold rolled sheets or in drawn wires. However, several factors can generate a break-up of this fibrous structure. A regular change in strain path, for example, seems to be very effective in generating a granular structure, with a mixture of HAB and LAB. Large non-deformable particles cause inhomogeneous deformation of the adjacent matrix and destroy the planarity of the boundaries. Finally the formation of shear bands may cause significant displacements of the grain structure [26]. In fact, it seems that in materials with low stacking fault energy the refinement of the microstructure is realized via the formation of shear bands [5,27]. Most of the high angle boundaries retained after SPD have a non-equilibrium character [28,29]. A post-SPD thermal treatment may be necessary for certain applications. The thermal stability of these structures will be discussed in one of the following sections.

At elevated temperature grain subdivision is less extensive and the inhomogeneous deformation around particles is smaller [30]. New high angle boundaries are formed by a process called "geometrical dynamic recrystallization" [31]. During deformation, grain boundaries develop serrations with a wavelength similar to the subgrain size. When the original boundaries are sufficiently pressed together by the shape change of the grains, grain impingement occurs and an equiaxed fine-grained structure with a large number of high angle boundaries is formed.

### INFLUENCE OF STRAIN PATH

In most SPD processes (except HPT) the deformation is applied with repetitive changes in strain path. Especially in ECAP, several processing routes are available. The implications on the sample distortion have been described in detail by Furukawa et. al. [32] and are illustrated in fig. 4. A cubic element in the initial billet, is elongated into a rhombohedral shape during the first ECAP pass. The elongation is visible in the (XY) plane but not in the (YZ) plane. The first shear plane is active as indicated in fig 4a. When the second passage through the die is carried out without rotation (route A), a

further elongation in plane (XY) occurs. A second shear plane, perpendicular to the first (when  $\phi = 90^\circ$ ) is now active (fig. 4b). In further passes the  $1^\circ$  and  $2^\circ$  shear plane are alternating active and further elongation occurs in each pass. When route C is applied, (fig 4c), deformation always occurs along the same shear plane, but alternating in shear direction. The shape of an initial cubic element is restored after each 2N passes, with N an integer. In route B, the cubic volume element is elongated in each orthogonal plane after the  $2^\circ$  pass. For  $B_A$  this distortion will increase after each pass, but for route  $B_C$  the restoration of the cubic element is observed after each 4N passes. In the routes  $B_A$  and  $B_C$ , shear occurs on shear planes intersecting at  $120^\circ$ .

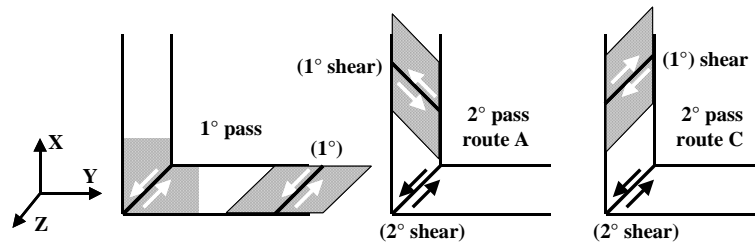


Fig. 4. Interactions of subsequent shear deformations in the first and second ECAP pass

In spite of the dynamic character of the (sub)structure development, the choice of processing route has a definite influence on the microstructure. Fig. 5 illustrates the elongated appearance of the microstructure after route A and the equiaxed nature after route C.

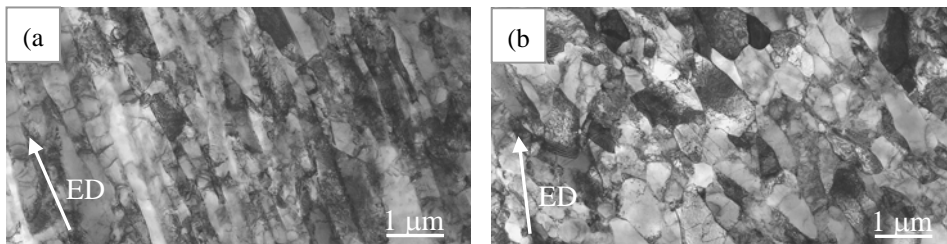


Fig. 5. TEM micrographs in plane XY of fig.4 of IF steel after 8 passes via (a) route A (b) route C. ED is the extrusion direction [33].

A further explanation for this has been provided by Dupuys et. al. [34]. They used the  $\alpha$  parameter introduced by Schmitt [35] to quantitatively express the change of strain path from one pass to another:

$$\alpha = \frac{\dot{\epsilon}_p \cdot \dot{\epsilon}}{\|\dot{\epsilon}_p\| \cdot \|\dot{\epsilon}\|} \tag{2}$$

with  $\dot{\epsilon}$  and  $\dot{\epsilon}_p$  the strain rate tensors of the consecutive passes. For the most drastic ‘orthogonal’ change in strain path,  $\alpha = 0$ . For a monotonous strain  $\alpha = 1$  and for strain reversal  $\alpha = -1$ . With the billet rotation in between two passes as a parameter, Dupuys found for different die angles of  $90^\circ$ ,  $120^\circ$  (or  $60^\circ$ ) and  $135^\circ$  (or  $45^\circ$ ), the  $\alpha$ -values shown in fig. 6. Route C corresponds in all cases to strain reversal. For route B  $-0.5 < \alpha < -0.25$  or in all cases “nearly” orthogonal. For route A however,  $\alpha$  is strongly

dependant on the ECAP die angle  $\phi$ . Dupuys assumed that the development of HAB during ECAP would be less efficient with more negative  $\alpha$ -values. Several experimental results published in literature seem to be in agreement with fig. 6. For a die angle of  $90^\circ$ , most papers (e.g. [36, 37] indicate that route B is more efficient than A and C, but it has also been reported that for a die with  $\phi = 120^\circ$  route A and B are nearly as effective but C is clearly less effective [38].

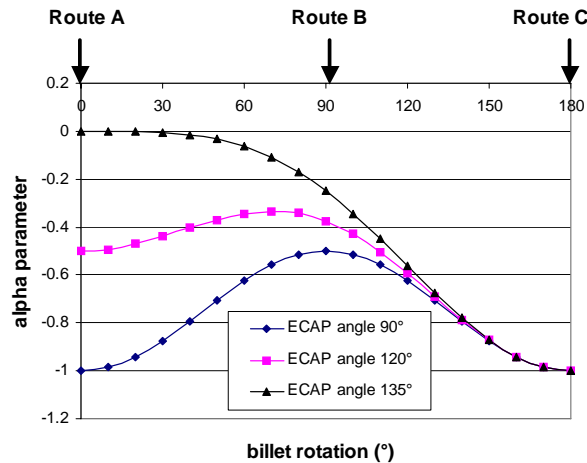


Fig. 6. Influence of ECAP-billet rotation on the  $\alpha$ -parameter defined in formula (2)

Not only the microstructure, but also the crystallographic texture of the samples is affected by SPD. Due to space limitations this topic will not be discussed further. For more information, the reader is referred to some recent studies [39,40,41].

### THERMAL STABILITY

The thermal stability of submicron materials formed by SPD is generally described as “relatively good” [42] or “reasonably stable” [43]. It does not mean that no microstructural changes will take place during post-SPD annealing. Fig. 7 shows the evolution of the structure of an AA1050 aluminium alloy, produced by 8 ECAP passes and annealed at  $300^\circ\text{C}$ . In the first stage, fig. 7(a), there is an overall coarsening of the substructure. Compared to the as ECAP’ed structure, the subgrains are more equiaxed and their size increased from  $1.2\mu\text{m}$  to  $2.2\mu\text{m}$ . In a second stage, fig. 7(b), some subgrains grow much faster than the surrounding structure. However abnormally growing grains, taking over the entire structure are not observed. In fig.7(c) and 7(d), after respectively 1h and 4h annealing at  $300^\circ\text{C}$ , clusters of subgrains are still visible between the larger grains.

The homogeneous coarsening of the structure, followed by discontinuous coarsening of some particular (sub)grains during annealing, has been observed by several other authors in aluminium alloys [28,29,43, 45] and IF steel [46]. There seems to be a common understanding that during the first stage of annealing, the (sub)structure formed during ECAP relaxes by recovery. The dislocation density inside the grains decreases, (sub)grain boundaries get a more equilibrated structure and some general (sub)grain coarsening occurs. The subsequent growth of some particular grains can be

understood in terms of Humphreys' "unified theory of recovery, recrystallization and grain growth" [47,48].

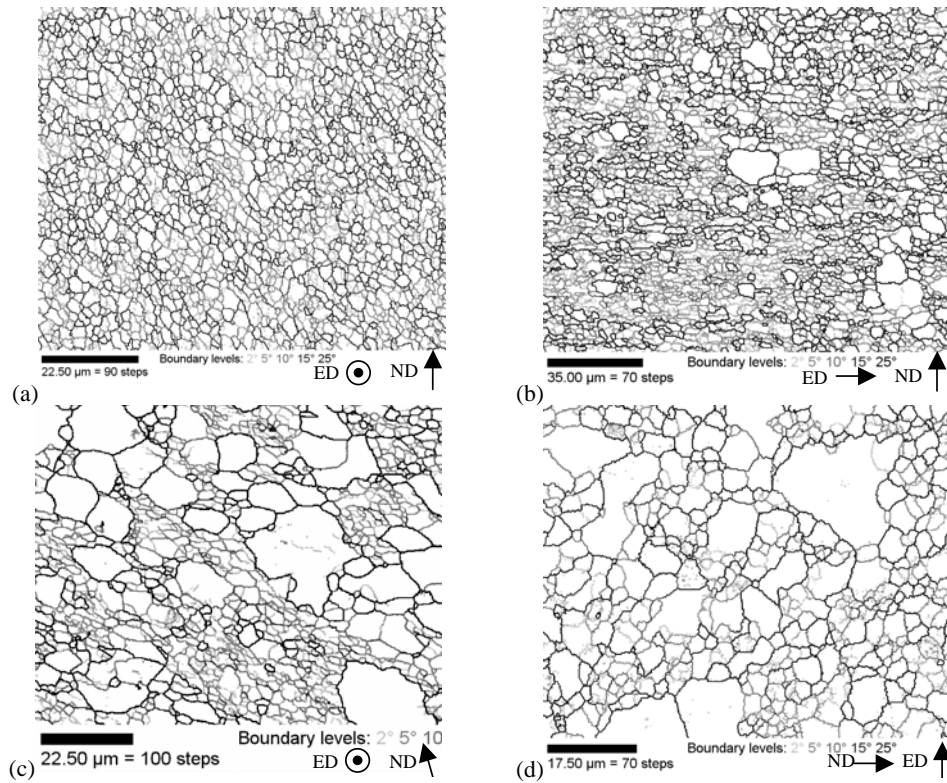


Fig. 7. Boundary plots of EBSD scans showing the microstructure evolution during annealing at 300°C of an 8pass ECAP sample of an AA1050 aluminium alloy: (a) 5 minutes, (b) 30 minutes, (c) 60 minutes, (d) 240 minutes [44]

### STRENGTH AND DUCTILITY

One of the major driving forces behind the development of submicron materials is their good strength/ductility balance. Fig. 8 shows that, as long as the total elongation in an uniaxial tensile test is considered, ECAP samples (8 passes route B<sub>c</sub>) have a better strength/ductility balance than the same material after different degrees of cold rolling. However, as reported by many investigators, ECAP material loses most of its strain hardening capacity (also shown in fig 10) and in a tensile test, the major part of the deformation is due to extensive post-uniform deformation. It's also worth mentioning that the high strength of ECAP samples is not 'abnormal'. Results from Horita et. al. [45] show that for an equivalent strain, the ECAP samples show the same strength as cold rolled material.



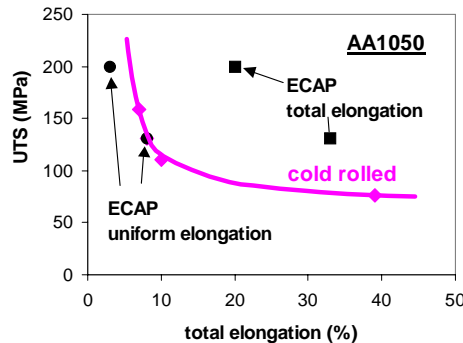


Fig. 8. Strength-ductility relation in uniaxial tension for ECAP material, compared to cold rolled material

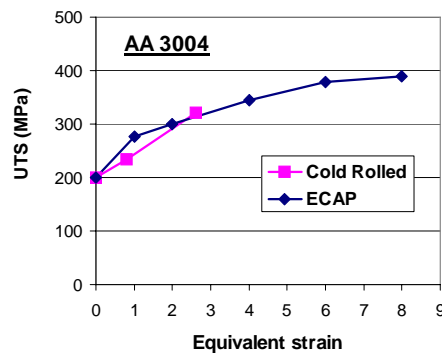


Fig. 9. Ultimate tensile strength for cold rolled and ECAP material as function of the applied strain [after 45]

Most mechanical data reported in literature are obtained by tension and/or compression tests. A complete picture of the flow behavior e.g. by a yield locus and the expansion of that yield locus with strain, has not yet been published. A first attempt has recently been reported by Poortmans [49], who measured the properties of as hot rolled, ECAP and post-ECAP annealed samples in tension, torsion and compression. For the hot rolled reference material the yield strength in tension and compression was nearly the same. The initial yield point  $\tau_y$  measured in torsion was equal to  $\sigma_y/\sqrt{3}$ . The yield surface of this hot rolled material can in a first approximation be described by an isotropic Von Mises yield locus or, when the (weak) texture is taken into account, by an anisotropic Hill yield locus. However, for the ECAP'ed material a clear tension/compression asymmetry in yield point was observed (200MPa against 163MPa). Such asymmetry has been reported before, but the data are conflicting. The yield strength of a Fe-10Cu alloy was 30% lower in tension than in compression [50], but for a SMG Fe the yield strength in tension was higher than in compression [51]. Yu et. al. [52] found for a AA1050 alloy, similar as the one used in the present study, a yield strength in tension of 152MPa and in compression of 185MPa. This yield point asymmetry is opposite to the one found in [49], where the yield strength in tension is 23% higher than in compression. In a phenomenological model, the asymmetry in

yielding can be taken into account with the incorporation of a back-stress [53]. The yield strength in torsion can then be calculated as  $(200\text{MPa} + 163\text{MPa})/2\sqrt{3} = 105\text{MPa}$ , in agreement with the experimental value of 107MPa.

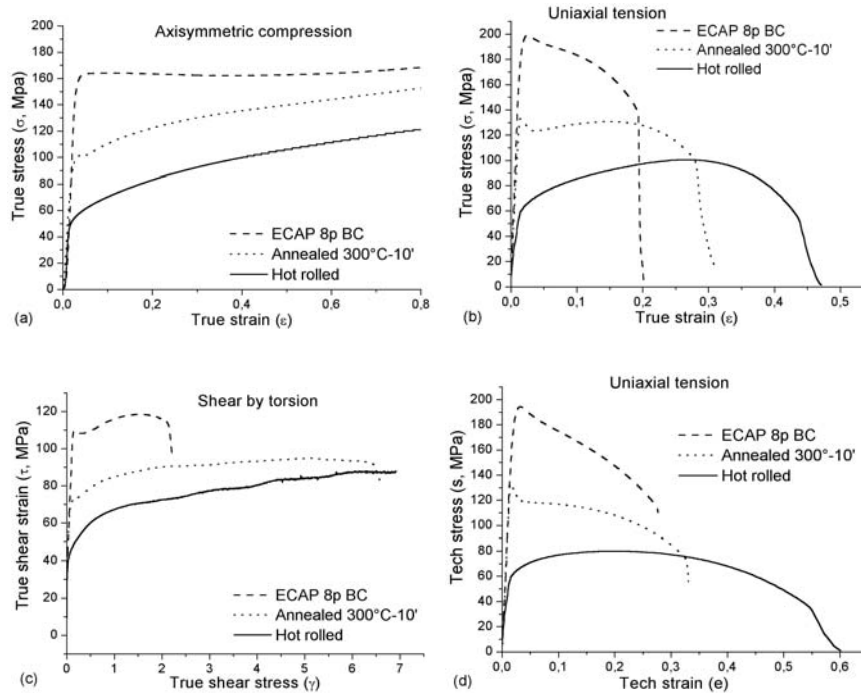


Fig. 10. Stress-strain curves for monotonic mechanical testing. (a) axisymmetric compression, (b) uniaxial tension (true stress, true strain), (c) simple shear by torsion (shear stress, shear strain) and (d) uniaxial tension (technical stress, technical strain) [49]

The strain hardening behavior of these materials is difficult to model, not only because of the occurrence of diffuse necking in a tensile test, but also because of a strong anisotropic yielding in compression tests (the circular cross sections become elliptic) and ‘transition’ effects (Lüder-like strain) between initial yielding and monotonous strain hardening. Further investigations on the effect of strain path changes are required to understand and model these transition effects.

### INTERACTION WITH PRECIPITATES

The current interest for the high strength level of submicron materials has prompted some research groups to explore the possibilities to combine substructure development with precipitation hardening, e.g. in precipitation hardenable Aluminium alloys. Murayama et. al. [54] investigated the precipitation process in an ECA-pressed Al-1.7at% Cu alloy. When aged samples were deformed by ECAP, the  $\theta'$  precipitates were fragmented and eventually dissolved. The hardness of those samples was lower than the hardness of single phase solution treated samples, even after one ECAP pass. When the solution treated samples were aged after ECAP, the equilibrium  $\theta$  phase was observed to nucleate at grain boundaries, suppressing the precipitation of GP-zones,  $\theta''$  and  $\theta'$  precursor phases. Mao et. al. [55] applied ECA pressing at 150°C and 190°C to an

AA2024 alloy in peak-aged and over-aged condition. In both conditions a significant grain refinement was obtained and the initial strength difference, due to the different ageing treatment, was preserved during ECAP. For the same alloy, Kang et. al. [56] reported a steady increase of hardness with increasing number of ECAP passes in over-aged samples and a gradual decrease for peak-aged samples, leading to equal hardness after 8 ECAP passes. The  $\theta'$  precipitates in the peak-aged samples were reported to dissolve during ECAP at 190°C. When samples were ECAP'ed in solutionized condition, a drastic increase in hardness was observed after 1 ECAP pass and a maximum hardness occurred after 3 passes. This increase in strength was attributed to dynamic precipitation. Similar investigations have been conducted in AA6xxx [57,58] and AA7xxx Aluminium alloys [59]. A possible synergetic effect between precipitation hardening and deformation during ECAP has been explored comparing a commercial AA5182 Al-Mg alloy and a modified variant with 1.2wt% Cu [60]. Although the alloy AA5182Cu was stronger than AA5182, the authors concluded that the precipitates formed during ECAP at 200°C, slow down recovery but do not contribute directly to the strength. It remains difficult to deduce a clear strategy for the most effective improvement of the strength of precipitation hardenable Aluminium alloys by ECAP, although the results of Kim et. al. on AA6061 [61] and AA2024 [62] suggest that a pre-ECAP solution treatment combined with a post-ECAP low temperature ageing is very effective.

### SUPERPLASTICITY

Superplasticity can be described as “the capability of a material to undergo very large plastic deformation”. In most cases superplasticity is obtained at high temperature (typically above  $0.5T_m$  with  $T_m$  the melting temperature in Kelvin) and low strain rate (typically  $10^{-3}/s$  or  $10^{-4}/s$ ). The main deformation mechanism is grain boundary sliding, but this sliding cannot occur without a diffusion controlled accommodation mechanism. This type of superplasticity is sometimes called “fine structure superplasticity”, because a small grain size (usually less than  $10\mu m$ ) is a necessary condition. Fig. 11 shows that at high strain rates, a classical dislocation glide mechanism (DISM) is active, but at low strain rates grain boundary sliding (GBS) is dominant. The same figure also shows the constitutive equations for both deformation mechanisms. A decrease in grain size shifts the stress – strain rate relation upward in the case of DISM and downward when GBS dominates. This shifts the domain where GBS is active, to higher strain rates. The production of submicron materials by SPD creates an opportunity to reduce the production time for superplastic forming (typically 20-30 minutes/part) with a factor 10 or more, which would open new markets for this forming technique. An alternative strategy is to reduce the deformation temperature. Several experimental results have been published, demonstrating the occurrence of high strain superplasticity and low temperature superplasticity.

High strain rate superplasticity (HSR-SP) is usually defined as superplastic deformation at a strain rate higher than  $10^{-2}/s$ . HSR-SP has been observed in the past, but in a restricted range of materials like some metal-matrix composites or some materials produced by powder metallurgy [63]. Valiev et. al. [64] have shown that HSR-SP can be obtained in two as-cast Al alloys after ECAP. In a classical Supral 100 alloy (Al-6Cu-0.4Zr) a grain size of  $0.5\mu m$  was obtained after 8 ECAP passes at 400°C and 4 passes at 200°C. Elongations of 970% at  $10^{-2}/s$  and 300°C or 740% at  $10^{-1}/s$  and 350°C

have been reported. With a Russian alloy 1420 (Al-5.5Mg-2.2Li-0.12Zr), subjected to the same ECAP scheme, a grain size of 1.2 $\mu$ m and elongations of 1180% at 10<sup>-2</sup>/s and 350°C, or 910% at 10<sup>-1</sup>/s were obtained. Even at a strain rate of 1/s (350°C), 350% elongation could still be reached. Further studies on this alloy showed that the optimum temperature for HSR-SP was 400°C with an elongation of 950% at a strain rate of 1/s [65].

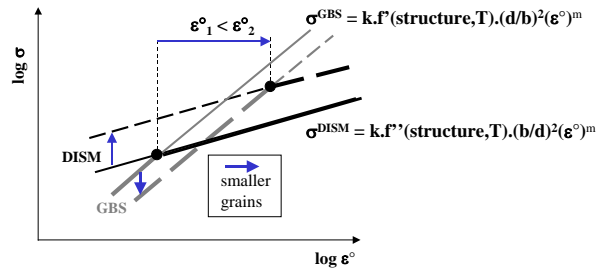


Fig. 11. Illustration of the influence of grain size ( $d$ ) on superplastic forming rates ( $\dot{\epsilon}^{\circ}$ ).  $T$  is the temperature,  $b$  de Burgers vector and  $\sigma^{DISM}$  and  $\sigma^{GBS}$  the stress needed to activate dislocation glide or grain boundary sliding

Another well investigated family of alloys are the Al-Mg-Sc alloys. In Al-3Mg-0.2Sc, a maximum elongation of 2280% was obtained at 400°C and 3.3 10<sup>-2</sup>/s with an initial grain size of 1.1 $\mu$ m. At a strain rate of 1/s still 210% elongation could be reached [66]. Further investigations on this alloy [67] revealed that a microstructure of equiaxed grains, separated by high angle boundaries is a prerequisite for superplasticity (grain boundary sliding). This was achieved most readily using ECAP route B<sub>C</sub>. For example after 8 ECAP passes route B<sub>C</sub>, tensile testing at 400°C and strain rate 3.3 10<sup>-2</sup>/s provides elongations around 2000%, while after pressing following route A or C only 1500% elongation is recorded [67]. Since in most industrial superplastic forming operations thin sheets are used, some as-pressed ECAP samples have been cold rolled at RT to 2.2mm. This material was then tested and it appeared that it had not lost its excellent superplastic properties, despite the slightly elongated grains that developed during cold rolling [68]. In variants with higher Mg content, HSR-SP has also been recorded, e.g. in Al-6Mg-0.3Sc-0.3Mn, were elongations-to-failure up to 2000% have been observed at 450°C and an initial strain rate of 5.6 10<sup>-2</sup>/s [69].

Those studies also showed that very fine grains are not a sufficient condition to achieve HSR-SP. The fine grains must be stable enough to withstand coarsening at the high deformation temperatures. For example, the grain size in classical Al-Mg alloys (AA5xxx), can very efficiently be refined by SPD, but at superplastic deformation temperatures those grains are not stable enough to withstand (dynamic) grain growth. For this reason the alloys used for superplastic applications contain fine dispersoids that slow down or inhibit grain growth. In the Supral 100 alloy Al<sub>3</sub>Zr particles are present and in the Russian alloy 1420,  $\beta'$ -Al<sub>3</sub>Zr and  $\delta'$ -Al<sub>3</sub>Li; in the Al-3Mg-0.2Sc alloy pinning of grain boundaries is provided by Al<sub>3</sub>Sc particles. HSR-SP has been reported in several other alloys, e.g. in a spray cast Al-7034 [70], a number of Mg alloys [71] and in a commercial AA2024 alloy [72].

The very fine grain size provided by SPD, can also be used to lower the superplastic deformation temperature, at the expense of the higher strain rate. When

superplastic deformation is carried out below  $0.5T_m$ , we speak about “low temperature superplasticity” (LT-SP).

### FATIGUE

The fatigue properties of fine grained materials have less intensely been studied than their static strength properties. In general it is observed that the high cycle fatigue (HCF) life of most SPD materials is enhanced compared to their coarse grained counterparts [73,74]. In HCF the elastic component of the strain amplitude is dominant and the fatigue life is dictated by the fracture strength of the material, so that in general the fatigue limit of the material increases with increasing strength [73], which is in favor of SPD materials. In low cycle fatigue on the other hand, the fatigue resistance of conventional coarse grained materials, is in general superior to that of SPD material. This is schematically shown in fig. 12. The total strain amplitude ( $\Delta\epsilon_t/2$ ) can be divided in an elastic part and a plastic part. The elastic part, related to HCF, can in general be expressed by the Basquin law in function of the fatigue strength  $\sigma'_f$ , the Young's modulus  $E$ , the fatigue strength exponent  $b$  and the number of cycles  $N_f$ . The plastic part, related to LCF, is expressed by the Coffin-Manson relation, with  $\epsilon'_f$  the fatigue ductility and  $c$  the fatigue ductility coefficient (with  $c > b$ ):

$$\Delta\epsilon_t/2 = \Delta\epsilon_e/2 + \Delta\epsilon_p/2 = (2N_f)^b (\sigma'_f/E) + \epsilon'_f (2N_f)^c \quad (3)$$

In a  $\log(\Delta\epsilon_t/2)$  versus  $\log(2N_f)$  plot, both relations are represented by a straight line (fig. 12). For low number of cycles the plastic part of the strain amplitude is much larger than the elastic part, but for a large number of cycles the elastic part is dominant. When a material with conventional grain size is now deformed by SPD, the strength in general (also  $\sigma'_f$ ) will increase and the ductility ( $\epsilon'_f$ ) will decrease, shifting the fatigue curve downward for LCF and upward for HCF.

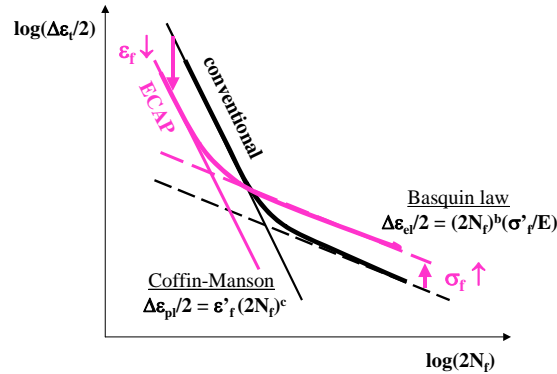


Fig. 12. Schematic illustration of the influence of ECAP deformation on the fatigue life of a material (adapted from Mughrabi [74])

It has been suggested [75] that the reduced fatigue resistance in LCF is mainly due to the susceptibility to strain localization of ECAP material. Hence it is reasonable to expect an enhancement of LCF properties after a short annealing treatment. This has indeed been observed in a number of alloys like AA5056 [75] or Cu [76]. Unfortunately

an improvement in LCF goes hand in hand with a decrease in HCF resistance. Hence, for each application a suitable balance between both must be found.

### **CORROSION**

The corrosion behavior of ultrafine grained materials has received only limited attention in published literature and it is difficult to formulate general conclusions at this moment. Thorpe et. al. [77] have shown that for nanostructured materials (not made by SPD) enhanced corrosion properties in comparison with coarse grained variants may be possible. On the other hand, Rofagha et. al. observed no difference in corrosion resistance between nanocrystalline pure Ni and its coarse grained counterparts [78] and a degradation in corrosion resistance was even reported for fine grained Ni-P [79].

For a 99.6% Cu with a grain size of 200 nm produced by ECAP, it was observed that the corrosion behavior had not qualitatively changed [80], but later [81] a better stress corrosion resistance was reported. For a Ti alloy an increase in corrosion resistance in HCl and H<sub>2</sub>SO<sub>4</sub> solutions after 8 ECAP passes, route B<sub>C</sub>, was observed. This improvement was related to the rapid formation of passive films at surface crystalline defects like grain boundaries and dislocations [82]. In a commercial purity Al (AA1050) the corrosion resistance was investigated in function of increasing number of ECAP passes and it was clearly shown that the resistance against pitting corrosion improved with increasing number of passes [83]. This was related to the decreasing size of Si-containing impurities. They formed local galvanic cells, which decreased in area with increasing ECAP passes.

### **CONCLUSIONS**

Fine grained materials produced by SPD can be generated on a laboratory scale in an effective and simple way, e.g. by ECAP or HPT. Up-scaling of those techniques is not evident, but interesting adaptations of the ECAP technique, like conshearing, continuous confined strip shearing and ECAP-conform, are being developed. Possible alternatives are ARB, asymmetric rolling or corrugation and straightening. The main lines of substructure and fine grain formation are more or less understood, although several details need some further clarifications. The thermal stability of those submicron structures is good, although some grain coarsening, followed by the development of a bimodal grain size distribution is observed. Important mechanical properties, like strength and ductility are intensely studied, but a complete picture of yield behavior (yield locus) and strain hardening (including changes in strain path) is still missing. SPD opens for many materials new possibilities for high strain rate and/or low temperature superplasticity, although this requires alloy compositions that can guarantee an adequate thermal stability. The fatigue properties of fine grained materials have less intensely been studied than their static strength properties. In general it is observed that the high cycle fatigue life of most SPD materials is enhanced compared to their coarse grained counterparts, but low cycle fatigue is less good. The results of corrosion tests are less abundant and not yet conclusive.

### **ACKNOWLEDGEMENTS**

Part of this work was carried out in the frame of the 'Interuniversity Attraction Poles Program - Belgian Science Policy' under contract number P5-08. We also

acknowledge the support from the Belgian Science Foundation (FWO) under contract number G.0208.02.

#### REFERENCES

- [1] E.O. Hall, Proc. Phys. Soc. London, 643 (1951), 747-753
- [2] N.J. Petch, J. Iron Steel Inst. London, 173 (1953), 25
- [3] G. Langford and M. Cohen, Trans. ASM, 62 (1969), 623-638
- [4] J. Gill Sevillano, P. Van Houtte and E. Aernoudt, Progr. Mat. Sci., 25 (1980), 69-412
- [5] R.Z. Valiev, R.K. Islamgaliev and I.V. Alexandrov, Progr. Mat. Sci., 45 (2000) 103-189
- [6] V.M. Segal, V.I. Reznikov, A.E. Drobyshevskij and V.I. Kopylov, Metally 1 (1981), 115
- [7] V.M. Segal, Mater. Sci. Eng., A197 (1995), 157-164
- [8] H.S. Kim, M.H. Seo and S.I. Hong, Mater. Sci. Eng., A291 (2000), 86-90
- [9] H.S. Kim, M.H. Seo, S.I. Hong, H.R. Lee, B.S. Chun and K.H. Lee, Mater. Sci. Forum, 386-388 (2002), 421-426
- [10] A. Gholinia, P. Bate and P.B. Prangnell, Acta Materialia, 50 (2002), 2121-2136
- [11] Y. Iwahashi, J. Wang, Z. Horita, M. Nemoto and T.G. Langdon, Scripta Metall. 35 (1996), 143-146
- [12] R.E. Barber, T. Dudo, P.B. Yasskin and T. Hartwig, in "Ultrafine Grained Materials III", ed. Y.T. Zhu et. al., TMS, 2004, 667-672
- [13] Y. Saito, H. Utsunomiya, H. Suzuki and T. Sakai, Scripta Mater. 42 (2000), 1139-1144
- [14] J.C. Lee, H.K. Seok and J.Y. Suh, Acta Mater. 50 (2002), 4005-4019
- [15] G.J. Raab, R.Z. Valiev, T.C. Lowe and Y.T. Zhu, Mater. Sci. Eng., A382 (2004), 30-34
- [16] Y. Saito, N. Tsuji, H. Utsunomiya, T. Sakai and R.G. Hong, Scripta Mat. 39 (1998), 1221-1227
- [17] N. Tsuji, N. Kamikawa, H.W. Kim and Y. Minamino, in "Ultrafine Grained Materials III", ed. Y.T. Zhu et. al., TMS, 2004, 219-226
- [18] L. Kestens, A. Carmen C. Reis, Y. Houbaert, in "Ultrafine Grained Materials III", ed. Y.T. Zhu et. al., TMS, 2004, 285-290
- [19] Q. Cui and K. Ohori, Mater. Sci. Techn. 16 (2000), 1095-1101
- [20] J.Y. Huang, Y.T. Zhu, H. Jiang and T.C. Lowe, Acta Mater. 49 (2001), 1497-1505
- [21] D.H. Shin, J.J. Park, Y.S. Kim and K.T. Park, J. Mater. Sci. Eng. 328 (2002), 98-103
- [22] J.W. Lee and J.J. Park, J. Mater. Proc. Techn. 130-131 (2002), 208-213
- [23] C.S. Barrett and L.H. Levenson, Trans. AIME 137 (1940), 112

- [24] D.A. Hughes and N. Hansen, *Acta Mater.* 45 (1997), 3871-3886
- [25] B. Bay, N. Hansen, D.A. Hughes, and D. Kuhlmann-Wilsdorf, *Acta Metall. Mater.* 40 (1992), 205-219
- [26] F.J. Humphreys, P.B. Prangnell, J.R. Bowen, A. Gholinia and C. Harris, *Phil. Trans. R. Soc. London A357* (1999), 1663-1681
- [27] K. Higashida and T. Morikawa, in "Nanomaterials by Severe Plastic Deformation", ed. M.J. Zehetbauer and R.Z. Valiev, Wiley-VCH, 2004, 517-522
- [28] J. Wang, Y. Iwahashi, Z. Horita, M. Furukawa, M. Nemoto, R.Z. Valiev and T.G. Langdon, *Acta Mater* 44 (1996), 2973-2982
- [29] D.G. Morris and M.A. Munoz-Morris, *Acta Mater* 50 (2002), 4047-4060
- [30] F.J. Humphreys and M. Hatherly, *Recrystallization and Related Annealing Phenomena*, Pergamon, 1996
- [31] H.J. McQueen, O Knustad, N. Ryum and J.K. Solberg, *Scripta Metall.* 19 (1985), 73-78
- [32] M. Furukawa, Z. Horita, M. Nemoto and T.G. Langdon, *J. Mater. Science* 36 (2001), 2835-2843
- [33] J. De Messemaeker, B. Verlinden and J. Van Humbeeck, in "Ultrafine Grained Materials III", ed. Y.T. Zhu et. al., TMS, 2004, 595-600
- [34] L. Dupuy and E.F. Rauch, *Mater. Sci. Eng. A337* (2002), 241-247
- [35] J.H. Schmitt, E. Aernoudt and B. Baudelet, *Mater. Sci. Eng.* 75 (1985), 13-20.
- [36] T.G. Langdon, M. Furukawa, Z. Horita and M. Nemoto, in "Investigations and Applications of Severe Plastic Deformation" Kluwer Academic Publisher 2000, 149-154
- [37] K. Oh-Ishi, Z. Horita, M. Furukawa, M. Nemoto and T. Langdon, *Metall. Mater. Trans.* 29A (1998), 2011-
- [38] A. Gholinia, P.B. Pragnell and M.V. Markushev, *Acta Mater.* 48 (2000), 1115-1130.
- [39] L.S. Toth, R. Arruffat Massion, L. Germain, S.C. Baik and S. Suwas, *Acta Mater.* 52 (2004), 1885-1898
- [40] S. Li, I.J. Beyerlein and M. Bourke, *Mater. Sci Eng. A*, (2005), in press
- [41] S. Li, I.J. Beyerlein, D.J. Alexander and S.V. Vogel, *Acta Mater.* 53 (2005), 2111-2125
- [42] Y.T. Zhu and T.G. Langdon, *JOM* 56 (10) (2004), 58-63
- [42] W.Q. Cao, A. Godfrey, W. Liu, Q. Liu, *Materials Letters*, 57 (2003), 3767-3774
- [44] S. Poortmans and B. Verlinden, *Mater. Sci. Forum*, 467-470 (2004), 1319-1324
- [45] Z. Horita, T. Fujinami, M. Nemoto and T. G. Langdon, *Metall. Trans.* 31A (2000), 691-701
- [46] J. De Messemaeker, J. Van Humbeeck and B. Verlinden, *Mater. Sci. Forum*, 467-470 (2004), 1295-1300
- [47] F.J. Humphreys, *Acta Materialia* 45 (1997), 4231-4240
- [48] F.J. Humphreys, *Acta Materialia* 45 (1997), 5031-5039



- [49] S. Poortmans and B. Verlinden, Proc. 3th Int. Conf. On Nano-SPD, Fukuoka, sept. 2005
- [50] J.E. Carsley, A. Fisher, W.W. Miligan and E.C. Aifantis, Metall Mater Trans A, 29 (1998), 2261-2271
- [51] B.Q. Han, E.J. Lavernia, and F.A. Mohamed, Metall Mater Trans A, 34 (2003), 71-83
- [52] C.Y. Yu, P.L. Sun, P.W. Kao and C.P. Chang, Scr. Mat., 52 (2005), 359-363
- [53] W. Prager, J. Applied Phys., 20 (1949), 235-241
- [54] M. Murayama, Z. Horita and K. Hono: Acta Mater. 49 (2001), 21-29
- [55] J. Mao, S.B. Kang and J.O. Park: J. Mater. Process. Tech. 159 (2005), 314-320
- [56] S.B. Kang, C.Y. Lim, H.W. Kim and J. Mao: Mat. Sci. Forum 396-402 (2002), 1163-1168
- [57] I. Gutierrez-Urrutia, M.A. Munoz-Morris and D.G. Morris: Mat. Sci. Eng. A-Struct., in press (available in [www.sciencedirect.com](http://www.sciencedirect.com))
- [58] J.K. Kim, H.G. Jeong, S.I. Hong, Y.S. Kim and W.J. Kim: Scripta Mater. 45 (2001), 901-907
- [59] Y.H. Zhao, X.Z. Liao, Z. Jin, R.Z. Valiev and Y.T. Zhu: Acta Mater. 52 (2004), 4589-4599
- [60] B. Verlinden and M. Popovic, Proc. 3th Int. Conf. On Nano-SPD, Fukuoka, sept. 2005
- [61] W.J. Kim, J.K. Kim, T.Y. Park, S.I. Hong, D.I. Kim and Y.S. Kim: Metall. Mater. Trans. A 33 (2002), 3155-3164
- [62] W.J. Kim, C.S. Chung, D.S. Ma, S.I. Hong and H.K. Kim: Scripta Mater. 49 (2003), 333-338
- [63] K. Higashi, M. Mabuchi and T.G. Langdon, ISIJ Int. 36 (1996), 1423-1438
- [64] R.Z. Valiev, D.A. Salimonenko, N.K. Tsenev, P.B. Berbon and T.G. Langdon, Scripta Mater. 37 (1997), 1945-1950
- [65] S. Lee, P.B. Berbon, M. Furukawa, Z. Horita, M. Nemoto, N.K. Tsenev, R.Z. Valiev and T.G. Langdon, Mater. Sci. Eng. A272 (1999), 63-72
- [66] Z. Horita, M. Furukawa, M. Nemoto, A.J. Barnes and T.G. Langdon, Acta Mater. 48 (2000), 3633-3640
- [67] S. Komura, M. Furukawa, Z. Horita, M. Nemoto and T.G. Langdon, Mater. Sci. Eng. A297 (2001), 111-118.
- [68] H. Akamatsu, T. Fujinami, Z. Horita and T.G. Langdon, Scripta Mater. 44 (2001), 759-764
- [69] F. Musin, R. Kaibyshev, Y. Motohashi and G. Itoh, Scripta Mater. 50 (2004), 511-516
- [70] C. Xu, M. Furukawa, Z. Horita and T.G. Langdon, Acta Mater. 51 (2003), 6139-6149
- [71] Z. Horita, K. Matsubara, Y. Miyahara and T.G. Langdon, "Nanomaterials by Severe Plastic Deformation", ed. M.J. Zehetbauer and R.Z. Valiev, Wiley-VCH, 2004, 711-716

- [72] C. Xu, M. Furukawa, Z. Horita and T.G. Langdon, "Nanomaterials by Severe Plastic Deformation", ed. M.J. Zehetbauer and R.Z. Valiev, Wiley-VCH, 2004, 701-710
- [73] A. Vinogradov and S. Hashimoto, "Nanomaterials by Severe Plastic Deformation", ed. M.J. Zehetbauer and R.Z. Valiev, Wiley-VCH, 2004, 663-676
- [74] M. Mughrabi, H.W. Höppel and M. Kautz, *Scripta Mater.* 51 (2004), 807-812
- [75] V. Patlan, A. Vinogradov, K. Higashi and K. Kitagawa, *Mater. Sci. Eng. A300* (2001), 171-182
- [76] A. Vinogradov, *Scripta Mater.* 39 (1998), 797-805
- [77] S.J. Thorpe, B. Ramaswami and A.T. Aust, *J. Electrochem. Soc.* 135 (1988), 2162-2170
- [78] R. Rofagha, R. Langer, A.M. El-Sherik, U. Erb, G. Palumbo and K.T. Aust, *Scripta Metall.* 25 (1991), 2867-2672
- [79] R. Rofagha, U. Erb, D. Olander, G. Palumbo and K.T. Aust, *Nanostruct. Mater.* 2 (1993), 1
- [80] A. Vinogradov, T. Mimaki, S. Hashimoto and R. Valiev, *Scripta Mater.* 41 (1999), 319-326
- [81] T. Yamasaki, H. Miyamoto, T. Mimaki, A. Vinogradov and S. Hashimoto, *Mater. Sci. Eng. A318* (2001), 122-128
- [82] A. Balyanov, J. Kutnyakova, N.A. Amirkhanova, V.V. Stolyarov, R.Z. Valiev, X.Z. Liao, Y.H. Zhao, Y.B. Jiang, H.F. Xu, T.C. Lowe and Y.T. Zhu, *Scripta Mater.* 51 (2004), 225-229
- [83] M.K. Chung, Y.S. Choi, J.G. Kim, Y.M. Kim, J.C. Lee, *Mater. Sci. Eng. A366* (2004), 282-291